Proceedings of the 2009 IEEE International Conference on Systems, Man, and Cybernetics
San Antonio, TX, USA - October 2009

A Novel Approach To Video-Based Pupil Tracking

Nishant Kumar
Dept. of Mechanical Engineering
IIT Bombay
Mumbai, India
nishantkumar@iitb.ac.in

Stefan Kohlbecher[1], Erich Schneider[2]
Clinical Neurosciences
University of Munich Hospital
Munich, Germany
[1]skohlbecher@nefo.med.uni-muenchen.de
[2]ESchneider@nefo.med.uni-muenchen.de

***Abstract*— EyeSeeCam is a novel head mounted camera that is continuously oriented to the user's point of regard by the eye movement signals of a mobile video-based eye tracking device. We have devised a new eye tracking algorithm for EyeSeeCam which has low computational complexity and lends enough robustness in the detection of pupil centre. Accurate determination of the location of the centre of the pupil and processing speed are the most crucial requirements in such a real-time video-based eye-tracking system. However, occlusion of the pupil by artifacts such as eyelids, eyelashes, glints and shadows in the image of the eye and changes in the illumination conditions pose significant problems in the determination of pupil centre. Apart from robustness and accuracy, real-time eye-tracking applications demand low computational complexity as well. In our algorithm, the Fast Radial Symmetry Detector is used to give a rough estimate of the location of the pupil. An edge operator is used to produce the edge image. Unwanted artifacts are deleted in a series of logical steps. Then, Delaunay Triangulation is used to extract the pupil boundary from the edge image, based on the fact that the pupil is a convex hull. A luminance contrast filter is used to obtain an ellipse fit at the sub-pixel level. The ellipse fitting function is based on a non iterative least squares minimization approach. The pupil boundary was detected accurately in 96% of the cases, including those in which the pupil was occluded by more than half its size. The proposed algorithm is also robust against drastic changes in the environment, i.e., eye tracking in a closed room versus eye tracking in sunlight.**

***Keywords*— mean-luminance filter, fast radial symmetry detector, edge detection, delaunay triangulation, luminance contrast filter, sub-pixel ellipse fitting**

I. INTRODUCTION

An eye tracking system measures the point of gaze, i.e., "where we are looking at" or the movement of the eye relative to the head. We have devised a novel eye tracking algorithm which has low computational complexity and lends enough robustness in the detection of pupil centre, fit to be used reliably in an eye tracking system. The algorithm is tailored to be applied on the video recorded by EyeSeeCam at sampling rates higher than 300 Hz. EyeSeeCam is a novel head mounted camera that is continuously oriented to the user's point of regard by the eye movement signals of a mobile video-based eye tracking device [1-3]. Fig. 1 shows a subject wearing the EyeSeeCam.

Eye trackers can be used as an effective tool in several diagnostic and interactive applications. Diagnostic systems are used for research in the fields of neuroscience, visual system, psychology, cognitive linguistics, advertisements and ergonomics. Eye tracking methods have been used for the diagnosis of diseases associated with vertigo and other neurological disorders which include studies such as the neurophysiological investigation of illusory contours or the investigation of the neuronal activity related to fixational eye movements thereby monitoring brain activity as well as oculomotor function concurrently [4-6]. Assessment of the gain and phase of the angular vestibulo-occular reflex (aVOR), which precisely compensates for head movements to maintain the eyes stable in space for visual acuity while moving also, requires an accurate determination of eye-orientation [7-9]. Systems which unite functional brain imaging and eye tracking have also been developed [10]. Tracking the eye-gaze has proved to be useful in studying human (overt) visual attention, for example while reading, scene perception, perception of art, perception of film and to analyze human visual search [11-14].

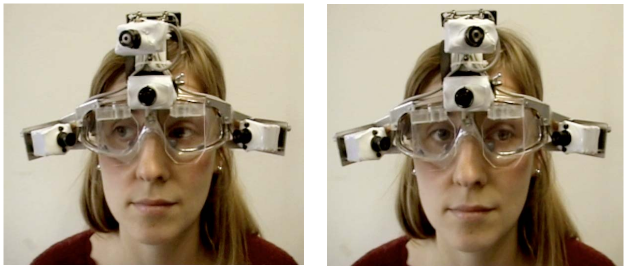

(a) (b)

Figure 1. A subject wearing the EyeSeeCam. In (a) the subject is looking towards her right and in (b) the subject is looking towards her left. Note that the head-camera at the top gets aligned along the gaze direction.

This study was supported by Deutsche Forschungsgemeinschaft (DFG: GL 342/1-3), and in part within the DFG excellence initiative research cluster Cognition for Technical Systems – CoTeSys.

978-1-4244-2794-9/09/$25.00 ©2009 IEEE

An interactive eye tracker serves as a powerful input device which finds applications in the field of Human-Computer Interaction, Visual Displays and Computer Graphics. A system based solely on gaze as input has been reported to be an important communication tool for quadriplegics, in which the eye is used to position a cursor on an oversized, projected keyboard [15]. Using gaze to assist in communication has been explored in multi-party computer supported collaborative work systems as well [16]. The knowledge of user's gaze can also be utilized to alter the display for speed-up purposes, as may be required in the rendering of complex virtual environments [17].

The most widely used eye tracking systems are video based, which use infrared video imaging of the pupil to determine 3D eye orientation [18-25]. The fundamental step is the determination of the pupil centre. Conventional approaches for this task include intensity based thresholding and computation of the centre of mass [18-21]. These approaches produce good results for fully visible and focused (ideal) images of the pupil. However, several artifacts such as eyelids, eyelashes, corneal reflections, shadows and reflections from the environment, and changes in illumination conditions pose significant challenges in the accurate determination of the pupil centre. With these practical problems in the hindsight, a curvature algorithm was proposed which uses the curvature characteristics of the pupil boundary to eliminate several unwanted artifacts [22]. In order to achieve robustness in an iris identification system, a Gaussian Mixture Model coupled with Kalman prediction of the pupil position along the sequence was also proposed [23]. A feature based probabilistic approach was attempted by exploiting the physiological properties of eyes as well as head/eye motion dynamics [24]. These approaches are however limited by speed and accuracy. Further development includes a hybrid eye tracking algorithm that integrates feature based and model based approaches [25].

The algorithm uses new techniques to obtain an accurate ellipse fit for the pupil at the sub-pixel level, as discussed in section 2. It is adaptive to even changes in the environment (inside the laboratory and out in the sun), and also to the variations in the features of the eyes for subjects belonging to different geographical locations, apart from the capability of handling the unwanted artifacts in the eye image efficiently. The algorithm was implemented in Matlab and the results obtained are presented in this paper.

II. Algorithm for Pupil Center Detection

The algorithm for the detection of pupil center operates on digital grayscale images. It employs a Fast Radial Symmetry Detector to give a rough estimate of the location of the pupil in the image [27]. An edge operator is applied on the image followed by morphological operations. Delaunay Triangulation is used to detect the boundary of the pupil [29]. Finally, the luminance contrast of the original image is used to obtain an ellipse fit at the sub-pixel level [30]. The steps involved in the algorithm are described in detail below.

A. Filtering the image

The grayscale image is filtered using a Mean Luminance (ML) Filter [26]. Mean Luminance is obtained by the convolution of the image by a Gaussian kernel as described by (1) and (2).

$$\mathrm{ML} = \mathrm{I} * \mathrm{G} \tag{1}$$

$$G = e^{-\left(\frac{x^2}{\sigma^2}+\frac{y^2}{\sigma^2}\right)} \tag{2}$$

The Gaussian Kernel is created using two parameters- *fwhm* (full width at half maximum) and the standard deviation σ. For a normal distribution, *fwhm* and standard deviation are related as in (3). The size of the kernel is also defined by *fwhm*.

$$fwhm = 2\sqrt{2\ln 2}\sigma \approx 2.35482\sigma \tag{3}$$

B. Estimating the pupil centre using the Fast Radial Symmetry Detector (FRSD)

FRSD is a point of interest detector which uses the image gradients to identify regions of high radial symmetry [26]. The computational complexity of FRSD is low and it also has faster runtimes, making it a useful tool for real-time vision systems [28]. It operates on a grayscale image and returns a 'symmetry map', i.e., bright points with high symmetry are marked with large positive values and dark points with high symmetry with large negative values. Since the pupil is the brightest part of an inverted image and has a high radial symmetry, FRSD helps in giving a first hint about the location of the pupil. The symmetry map obtained by applying it on an inverted image shows a bright patch at the pupil location. This symmetry map is further used to create a binary mask. The binary mask is multiplied with the inverted filtered image. This returns only those regions in the image which have high radial symmetry and are bright, as shown in Fig. 2.

The next step is to find the pupil amongst these regions. The different regions are picked up one-by-one and the average grayscale values of the pixels contained within that region is computed. Assuming that the brightest (since FRSD was applied on the inverted image) amongst these objects is the pupil, the region which scores the highest average value is taken to be a part of the pupil; hence the centroid of this region gives a first hint about the location of the pupil. In order to reduce computation, it is useful to diminish the region of interest. A square shaped mask is created around the estimated pupil centre and all the pixels which lie within this mask are retained while the others are discarded.

C. Edge detection

The Canny edge operator is applied to the original image to produce the edge image [31]. The pupil appears as a ring in the edge image. The eyelids, corneal reflections, shadows and eyelashes produce other significant edges. Our goal is to detect and isolate the pupil ring in the edge image.

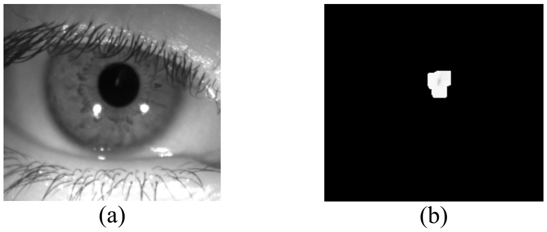

Figure 2. (a) Input image. (b) Symmetry map obtained by applying FRSD on the inverted input image. This is further used to obtain the binary map.

D. *Morphological operations*

For the later stages of the algorithm, it is essential to edit the edge image using simple morphological operations. These deletions are being performed in order to ensure that no artifact remains behind inside the pupil boundary, which would otherwise interfere with the triangulation algorithm to be described in the next section. These operations can be classified under the following two headings:

1) *Deleting glints*

The major source of a glint in the image is the beam of infrared rays used for video-oculography. In most of the frames, these prominent glints either lie inside the pupil, or on the pupil boundary. Fig. 3 shows the various possibilities of the location of these glints. In order that only the valid points enter the ellipse fitting function, it is important to delete the glints. Another source of glints is the reflection from the environment. These glints are generally faint and they do not form a closed ring in the edge image. These will be dealt with in the next section. In order to remove the prominent glints the following steps are followed.

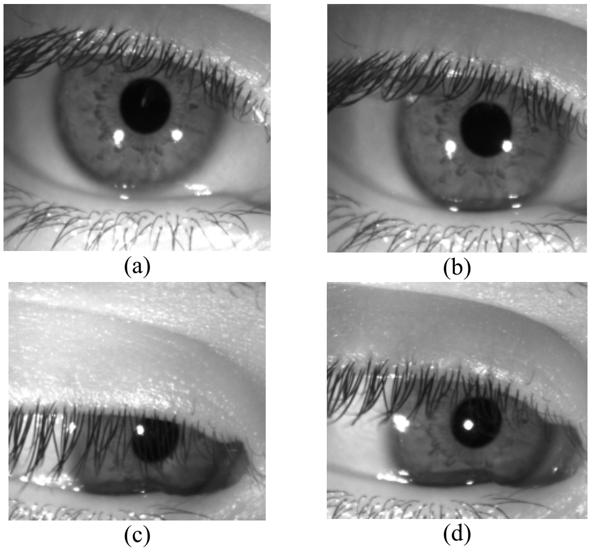

Figure 3. Location of glints on the pupil. (a) Glints outside the pupil completely, (b) Glint on the pupil boundary, (c) Glint on the inside boundary, (d) Glint completely inside the pupil.

We start with an edge image *A* and fill all the closed rings in this image to produce image *B*. *A* is subtracted from *B* to produce an image *C*. The next step is to extract the object from the image *C* which contains the pupil centre estimated by FRSD. Three possibilities arise here:

1. There is no such object. In this case image *C* is dilated, inverted and multiplied with image *A*.
2. Such an object exists but it is not the pupil itself. This means that the glint is inside the pupil boundary and the pupil boundary is an open ring. In this case also, the same procedure is repeated.
3. The pupil itself is the object. So we need to prevent the pupil from getting deleted. In this case, image *C* is eroded, inverted and then multiplied with image *A*. The resultant image is D. Images A, B, C and D are shown in Fig. 4.

This operation deletes all the closed rings in the edge image, except the pupil.

2) *Deleting the open ended chains*

One of the major difficulties in tracking the pupil boundary arises due to the eyelashes. In most of the frames, the eyelashes cover a major part of the pupil and mingle with the pupil boundary. It becomes even more difficult when the eyelashes of the subject are very dark. In the edge image, these appear as linear chains of white pixels. Another source of open ended chains is the faint glints, as introduced in the previous section. These do not form closed rings in the edge image, hence it becomes difficult to remove these in the same way as the prominent glints were removed. In order to overcome this problem, a very simple idea is used. All the open ended chains in the edge image are deleted based on the following two conditions:

a) The length of the chain to be deleted reaches a specified length, L_c. This specified length L_c, however, is not arbitrary. It is defined as a percentage of the number of pixels forming a non-occluded near perfect pupil.

b) While deleting the open-ended chain, if a point having three or more neighbors is reached and the upper limit to the number of points in the chain that can be deleted is not reached yet, then the chain deletion is stopped.

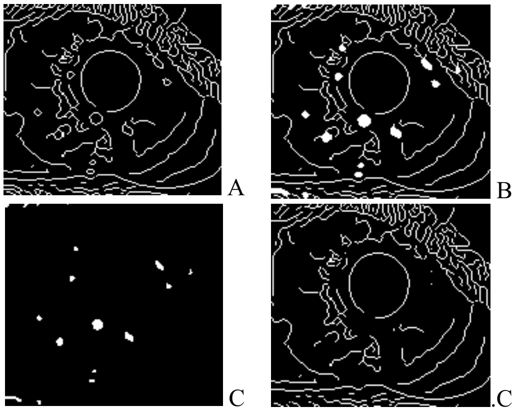

Figure 4. Images A, B, C and D involved in deleting the glints.

In order to implement this algorithm, the following steps are required. First of all, a *blue* image is created which contains only those points which have only one neighbor. These are the free ends of the open-ended chains. Now, each of these blue points is accessed sequentially and starting from such a point, the chain is traversed searching for neighbors in any of the eight cardinal directions as shown in Fig. 5. All the points that have already been traversed are colored *yellow.* Fig. 6 shows an image at an intermediate stage of processing, in which the *blue* and the *yellow* images have been superimposed. Fig. 6 shows three important cases that might arise in deciding what to remove and what not to remove. The free ends are shown as blue dots and the points already traversed are shown by yellow dots with a dash. The yellow chain in the centre of the image bounded by blue dots is a short open ended chain which satisfies the deletion criteria. There is another yellow chain which has a blue dot on one of its free ends while the other end terminates on to a point which has three neighbors. This again satisfies the deletion criteria. Lastly, there is a longer chain in the left part of the image. This chain does not satisfy the deletion criteria because it exceeds L_c , the specified length for chain deletion. Hence the chains which form a part of the pupil do not get deleted.

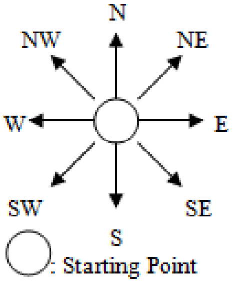

Figure 5. The figure above shows the eight cardinal directions in which the neighbouring points are accessed.

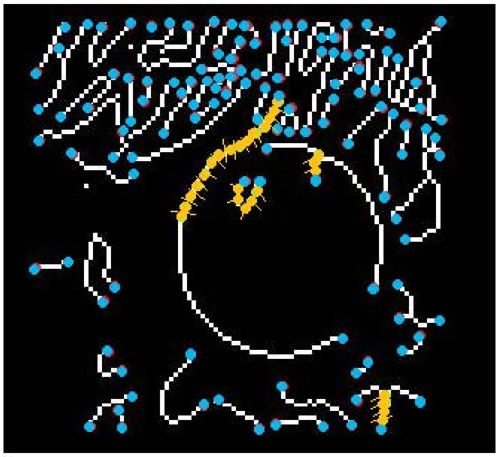

Figure 6. An intermediate stage in the algorithm while performing the morphological operations. The open ends of the open-ended chains are marked blue. The points already traversed are marked yellow with a dash.

E. Delaunay Triangulation for pupil boundary detection

After the necessary morphological operations have been performed, the next step is to find the pupil boundary. Delaunay Triangulation has been used for this task. It is an important tool for identifying a convex hull formed by a set of points in a 2D plane, which returns a set of triangles such that no data points are contained in any triangle's circumscribed circle. Delaunay triangulation has been extensively used for feature extraction in images [32-33]. The governing idea behind detecting the pupil using triangulation is the fact that pupil is also a convex hull. Triangulation is applied on all the white points in the edge image plus an additional point which is the estimated pupil centre. It splits up the image plane into numerous triangles as shown in Fig. 7, in which the pupil is distinctly identifiable as a convex structure. An important point to note in the triangulation is the fact that the triangles forming the pupil have one of their vertices lying on the estimated pupil centre. All the triangles with this property are extracted, because the remaining two vertices of these triangles lie on the pupil boundary. The advantage of using Delaunay Triangulation is that it automatically eliminates the unwanted artifacts on the pupil boundary as shown in Fig. 5. Here, the lines shown in red are actually the eye-lashes which have got fused with the pupil boundary. This can be verified by the input edge image shown in Fig. 8(a). The triangulation ignores these lines as they do not form a part of a convex hull. By picking up the points forming the vertices of the triangle lying on the pupil boundary, we are ignoring all those points which lie on an arc formed on the outer edge of the triangles. Hence a further step is required to collect all the valid points. For this, a very simple procedure is followed. The points obtained up to this stage are used as reference points and the neighbors of these points in the original edge image are picked up. Starting from one such reference point, the neighboring points are picked up until the next reference point is reached. However, if a free end is reached which is not one of the reference points; all the points collected in that chain are ignored. Hence, the pupil ring is extracted. The two stages of the pupil boundary extraction are shown in Fig. 8.

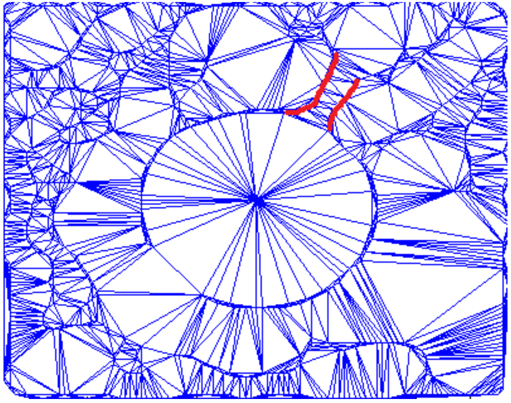

Figure 7. Delaunay Trianglulation is applied on the points forming the edge image. It splits the image plane into numerous triangles. All the triangles which have the estimated pupil centre as a common point amongst them are extracted. The red lines show that the trianguation discards all those parts in the edge image which do not form a convex hull.

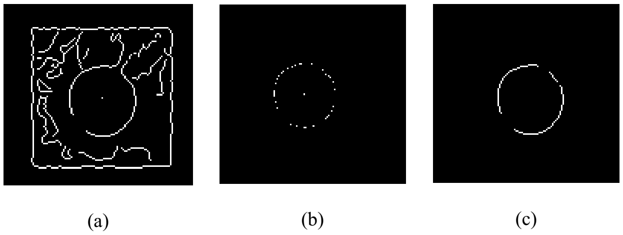

Figure 8. (a) Input edge image after morphological operations, (b) First stage of pupil boundary extraction, (c) Second stage of pupil boundary extraction. The triangulation shown in Fig. 7 is for Fig. 8(a) as input.

F. *Ellipse fitting at the sub-pixel level using the luminance contrast filter*

After all the valid points on the pupil boundary have been picked up, ellipse fitting is implemented. The ellipse fitting function used in the current implementation is based on a non-iterative least squares minimization approach [34], [35]. It is done in two stages. The first stage comprises ellipse fitting to the set of valid points obtained on the pupil boundary at a pixel level accuracy. To obtain the ellipse fit at the sub-pixel level, the luminance contrast filter is used [26], [30].

The luminance contrast of a local region is defined as the standard deviation of luminance in an isotropic patch around a point, which is further normalized by the mean luminance of the image [26]. The expression for luminance contrast is given as

$$LC = Re(\sqrt{(I^2*G) - (I*G)}) \div <I> \quad (4)$$

The filter produces a bright ring around regions of steep rise or fall of the grayscale value of the pixels. Since the pupil is considerably darker than the iris, the luminance contrast filter produces a distinct bright ring around the pupil as shown in Fig. 9(a). This bright ring is further used to obtain a sub-pixel level ellipse fit as described below.

Using the ellipse obtained in the first stage, two concentric ellipses are drawn which roughly serve as boundaries for the bright ring. From any point on the inner ellipse, the corresponding point on the outer ellipse is reached, while traveling in the direction of the normal to the ellipse at that point and ten points lying on this path are picked. The x and y coordinates of these ten points is weighted with the pixel values and the average is taken. The procedure is repeated for a large number of points on the ellipse. The points thus obtained are used for the final ellipse fit. The procedure is explained in Fig. 9(b). Fig. 9(c) shows the final ellipse fit obtained.

G. *Occlusion of the pupil by the upper eyelid*

The methods described above would fail to produce an accurate ellipse fit in the case when the pupil is occluded by the upper eyelid. This is because the triangulation treats the points of the eyelid boundary as points of the pupil boundary. In order to overcome this problem the following procedure is used. The pupil is said to be occluded by the upper eyelid when the length of the semi-minor axis, b, is less than 80% of the length of the semi-major axis, a, of the ellipse. The ellipse obtained for such a case is shown in Fig. 10 (a). Consider a similar ellipse shown in Fig. 10 (b). All the points lying above the major axis of this ellipse are discarded. A perpendicular bisector (AA') of the major axis is drawn and two points P1 and P2 are marked on this line. P1 is the point obtained by the intersection of the line AA' with the remaining segment BB' of the ellipse. The point P2 is marked such that the length of the line segment P1P2 is equal to the length of the minor axis of a non-occluded pupil obtained in the recently elapsed frames. Now, with all the points lying on the segment BB' and the point P2, a new ellipse is obtained which is much more accurate than the previously obtained ellipse. However, this step might not apply to eccentric eye positions, i.e. when the subject is looking towards extreme left or extreme right, because in this case, a situation might arise that both the axes are of comparable length and the pupil is still occluded.

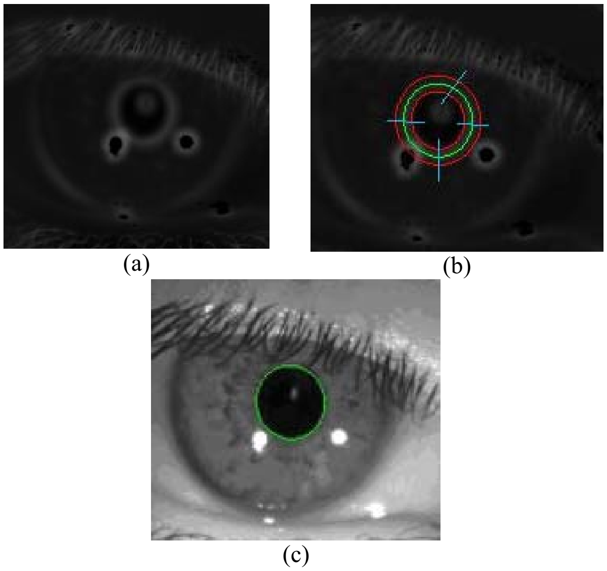

Figure 9. (a) The luminance contrast filter produces a bright ring around the pupil. (b) This image shows the procedure involved in obtaining the ellipse fit at the sub-pixel level. (c) The final ellipse fit on the pupil.

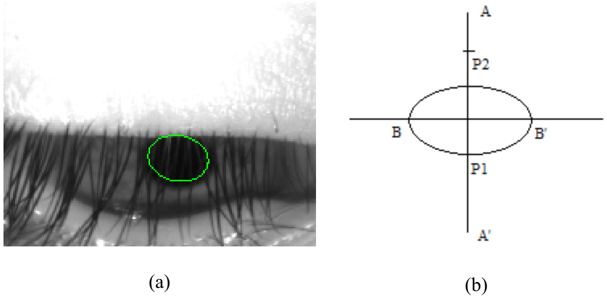

Figure 10. (a) Ellipse obtained in the case of occlusion by the upper eyelid. (b) A sketch showing the method adopted to improve the ellipse fit.

III. EXPERIMENTAL METHODS

Several videos were recorded using EyeSeeCam and stored in PGM file format. EyeSeeCam is a full featured binocular 3D video-based head-mounted eye-tracking system with a high spatial and temporal resolution [1-3]. The radius of the pupil changes with the amount of light it is exposed to. Hence, the pupil is very large in dark environments, and very small in areas of bright light. Keeping this in mind, some of the videos were taken in which the subjects were asked to explore freely inside the laboratory environment as well as in the sun outside. The videos comprised both: saccadic eye movements in free exploration as well as fixations at a point. The nature of the image of the eye obtained is important as well, which depends on the geographical background of the subject. Hence, videos of subjects of both Asian and European origin were recorded. The individual frames of these videos were accessed by indexing the PGM files.

IV. RESULTS

The performance of the algorithm can be assessed by analyzing a few parameters. The efficiency of FRSD in the present work can be defined as the error involved in the estimate of the pupil centre provided by FRSD and the resultant pupil centre obtained after the final ellipse fit. The standard deviation of this error was calculated to be 0.71 pixels. Pupil detection by the algorithm can be broadly classified into the following four possibilities:

True Positives: The pupil has been detected correctly.

True Negatives: The algorithm identifies that there was no pupil to be detected, e.g. eye closure.

False Positives: The algorithm detects a pupil where there is no such thing, e.g. dark eyelashes when the eye is closed.

False Negatives: The algorithm detects that there is no pupil even though there is a clearly visible pupil in the image.

Table 1 shows the percentage of such cases obtained.

We also need to quantify the ‘jitter’ in the location of the pupil centre as estimated by the algorithm in cases of eye fixations. The mean distance of the pupil centre from the mean pupil centre location (point of eye-fixation), was found to be 0.3 ± 0.07 pixels which corresponds to 0.1 ± 0.03° variation around the point of fixation. An important measure of robustness is the maximum percentage of occlusion under which the algorithm is able to return an accurate ellipse fit. In case of dark eyelashes of the subject, it becomes difficult to quantify the percentage of occlusion. However, we estimate that an accurate ellipse fit was obtained even when the pupil was hidden by the upper eyelid by more than half its size and also by eyelashes.

TABLE I. PUPIL DETECTION

S.No.	Types of pupil detection	Percentage
1	True Positives	93
2	True Negatives	3
3	False Positives	3
4	False Negatives	1

As far as the computational complexity is concerned, the analysis can be broken down to three segments. The first segment employs FRSD for the initial guess of the pupil location. It is fast and robust and operates with the order of computation of KN. Here, K is a constant and N is the number of pixel points on which the function operates. The second segment is the one where Delaunay Triangulation has been used for the detection of the pupil boundary. This triangulation is based on a randomized, incremental approach and operates with the order of computation of N log N. Ellipse fitting at the sub-pixel level is the third segment which involves a luminance contrast filter. This filter involves a 2-dimensional numerical convolution.

V. DISCUSSIONS

In this section we will discuss the results obtained in critical cases. The ellipse fitting of the pupil boundary is unaffected by the location of the glints and shadows in the image of the eye. Fig. 11 shows four such cases: (a) an unoccluded near perfect image of the pupil, (b) an image with two glints on the pupil boundary, (c) an image with one large glint on the pupil boundary and (d) an image with a glint inside the pupil boundary.

The pupil center detection is robust even with considerable changes in the illumination conditions of the environment as shown in Fig. 12. Fig. 12(a) shows the result obtained when the experiment was performed inside the laboratory room with normal lighting conditions. On the other hand, Fig 12(b) shows the result obtained when the subject stepped out of the laboratory for a free exploration in the sun. FRSD plays an important role in handling this aspect as it detects objects of high radial symmetry in the image. It takes as input, an estimate of the radius of the radially symmetrical object that we are interested in. Hence, by setting a very small radius, we can always ensure the detection of a disk fully contained within the pupil, which thereby helps us in arriving at an estimate of the location of the pupil.

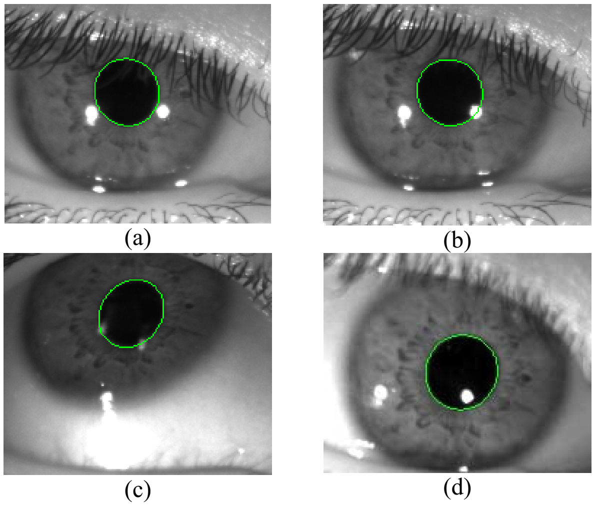
(a)

(b)

(c)

(d)

Figure 11. Ellipse fitting on the pupil for different locations of the glints.

The usefulness of Delaunay Triangulation for extracting the pupil boundary has already been described in the previous sections. Fig. 13(a) shows an ellipse fit over a pupil occluded heavily by eyelashes showing the effectiveness of the combination of morphological operations and triangulation. Fig. 13(b) shows the ellipse fit obtained in case of partial occlusion by the upper eyelid. The ellipse goes beyond the eyelid to capture the complete pupil boundary.

Spatial resolution is ascertained by ellipse fitting at the sub-pixel level using luminance contrast. Furthermore, all the tools used in the algorithm are computationally inexpensive, making it suitable for real time eye tracking applications. The main emphasis of this work was on enhancing the robustness of the algorithm for detecting the pupil boundary, paying lesser attention towards the processing speeds achieved. The algorithm has so far been developed and tested in Matlab.The next step would be to implement it in C and optimize the functions involved. Further improvements include using binomial filters in place of Gaussian filters which will further reduce the computational complexity. The methods described in this paper can also be applied to extract convex objects of interest from an image with accuracy.

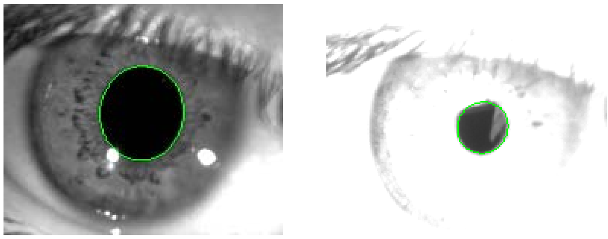

(a) (b)

Figure 12. (a) Ellipse fit obtained when the subject was inside the room. The size of the pupil is larger in this case. (b) Ellipse fit obatined when the subject was out in the sunlight. The size of the pupil is comparatively smaller in this case and the rest of the image is completely illuminated.

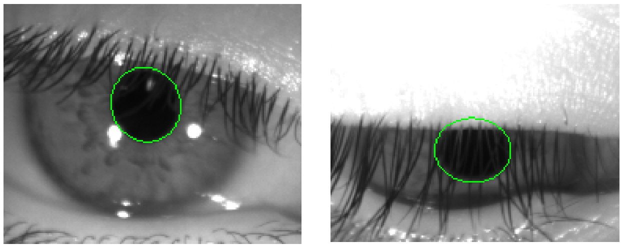

(a) (b)

Figure 13. (a) Ellipse fit obtained in the case of severe occlusion by the eyelashes. (b) Ellipse fit obtained in the case of occlusion by the eyelashes and also by the upper eyelid. Note that in this case the ellipse goes beyond the boundary of the upper eyelid.

Acknowledgment

This study was supported by Deutsche Forschungsgemeinschaft (DFG: GL 342/1-3), and in part within the DFG excellence initiative research cluster Cognition for Technical Systems – CoTeSys. N. K. thanks E. S. and other team members for their constant help and guidance all throughout this work.

References

[1] E. Schneider, K. Bartl, S. Bardins et al., "Eye movement driven head-mounted camera: It looks where the eyes look",2005, Proceedings of the IEEE International Conference on Systems, Man and Cybernetics : 2437–2442.

[2] E. Schneider, K. Bartl, S. Bardins et al., "Gaze-aligned head-mounted camera with pan, tilt, and roll motion control for medical documentation and teaching applications", 2006, Proceedings of the IEEE International Conference on Systems, Man and Cybernetics : 327–331.

[3] E. Schneider, K. Bartl, S. Bardins et al., "EyeSeeCam: An eye movement-driven head camera for the examination of natural visual exploration, in press.

[4] J. R. Leigh, D. S. Zee, The Neurology of Eye Movements, Davis, Philadelphia, 1983.

[5] D. A. Leopold and N. K. Logothetis, "Activity changes in early visual cortex reflect monkeys' percepts during binocular rivalry", Nature, 379, 1996, 549-553.

[6] I. Kagan, M. Gur, and D. M. Snodderly, "Spatial organization of receptive fields of V1 neurons of alert monkeys: comparison with responses to gratings", J Neurophysiol (November 1, 2002). 10.1152/jn.00858.

[7] T. Raphan, V. Matsuo, B. Cohen, "Velocity storage in the vestibulo-ocular reflex arc (VOR)", Exp. Brain Res. 35 (1979) 229–248.

[8] T. Raphan, B. Cohen, How does the vestibulo-ocular reflex work, in: R.W. Baloh, G.M. Halmagyi (Eds.), Disorders of the Vestibular System,Oxford University Press, New York, 1996, pp. 20–47.

[9] S. B. Yakushin, M. J. Dai, J. I. Suzuki, T. Raphan, B. Cohen, "Semicircular canal contribution to the three-dimensional vestibulo-ocular reflex: A model-based approach", J. Neurophysiol. 74 (1995) 2722–2738.

[10] J. Özyurt, P. DeSouza, P. West, R Rutschmann, M. W. Greenlee, 2001, "Comparison of cortical activity and oculomotor performance in the gap and step paradigms" Perception 30 ECVP Abstract Supplement.

[11] K. Rayner, "Eye movements in reading and information processing: 20 years of research", Psychological Bulletin 124 (1998), pp. 372–422.

[12] K. Rayner, T. J. Smith, G. L. Malcolm and J. M. Henderson, "Eye movements and visual encoding during scene perception", 2009, Psychological Science, 20, 6-10.2008.

[13] J. M. Henderson and A. Hollingworth, Eye movements, visual memory, and scene representation, In M. A. Peterson and G. Rhodes (Eds.), Analytic and holistic processes in the perception of faces, objects, and scenes, 2003, pp. 356-383, New York: Oxford University Press.

[14] J. Treuting, " Eye tracking and the cinema : A study of film theory and visual perception", SMPTE motion imaging journal ISSN 1545-0279, 2006, vol. 115, no1, pp. 31-40.

[15] A. T. Duchowski, Eye Tracking Methodology: Theory & Practice, Springer-Verlag, London, UK, 2nd edition, 2007. (ISBN: 1-84628-608-7).

[16] R. Vertegaal, "The GAZE Groupware System: Mediating Joint Attention in Multiparty Communication and Collaboration." In Proceedings of ACM CHI'99 Conference on Human Factors in Computing Systems. Pittsburgh, PA USA: ACM, 1999, ISBN: 0-201-48559-1 , pp. 294-301.

[17] B. H. McCormick, D. A. Batte and A. T. Duchowski, "A Virtual Environment: Exploring the Brain Forest", 1996, CENAC Conference, Mexico City, Mexico.

[18] P. Majaranta and K. Raiha, "Twenty years of eye typing: systems and design issues," in ACM Eye tracking research and applications symposium, New Orleans, Louisiana, USA, March 2002, pp. 15–22.

[19] A. H. Clarke, W. Teiwes, H. Scherer, Video-oculography— an alternative method for measurement of three-dimensional eye movements, in: R. Schmid, D. Zambarbieri (Eds.), Oculomotor Control and Cognitive Processes, Elsevier Science Publishers B. V., North-Holland, 1991, pp. 431–443.

[20] S. T. Moore, T. Haslwanter, I.S. Curthoys, S. T. Smith, “A geometric basis for measurement of three-dimensional eye position using image processing”, Vis. Res. 36 (1996) 445– 459.

[21] J. B. Mulligan, “Image processing for improved eye tracking accuracy”, Behav. Res. Methods, Instrum. Comput. 29 (1997) 54–65.

[22] D. Zhu, S. Moore, and T. Raphan, “Robust pupil center detection using a curvature algorithm,” Computer Methods and Programs in Biomedicine, 1999, vol. 59, no. 3, pp. 145–157.

[23] W. Ketchantang, S. Derrode, S. Bourennane and L. Martin, "Video Pupil Tracking for Iris Based Identification", Lecture Notes in Computer Science,Springer Berlin / Heidelberg, 2005, Vol. 3708/2005, ISSN: 0302-9743 (Print) 1611-3349 (Online).

[24] A. Haro, M. Flickner, and I. Essa, “Detecting and tracking eyes by using their physiological properties, dynamics, and appearance,” in IEEE Conference on Computer Vision and Pattern Recognition, June 2000, pp. 163–168.

[25] L. Dongheng, D. Winfield, D. J. Parkhurst, "Starburst: A hybrid algorithm for video-based eye tracking combining feature-based and model-based approaches", IEEE Computer Society Conference on Computer Vision and Pattern Recognition, 2005, Vol. 3 (2005), pp. 79-79.

[26] F. Schumann, W. Einhäuser, J. Vockeroth et al., "Salient features in gaze-aligned recordings of human visual input during free exploration of natural environments", 2008, J Vis : in press.

[27] G. Loy and A. Zelinsky, "Fast radial symmetry for detecting points of interest", 2003, IEEE Trans. Pattern Anal. Mach. Intell. 25(8): 959-973.

[28] L. Fletcher, G. Loy, N. Barnes, A. Zelinsky, "Correlating driver gaze with the road scene for driver assistance systems", 2005, Robotics and Autonomous Systems 52(1): 71-84.

[29] C. B. Barber, D.P. Dobkin, and H.T. Huhdanpaa, "The quickhull algorithm for convex hulls," ACM Transactions on Mathematical Software, Vol. 22, No. 4, Dec. 1996, p. 469-483.

[30] J. Zhu and J. Yang, “Subpixel eye gaze tracking,” IEEE Conference on Automatic Face and Gesture Recognition, May 2002, pp. 124–129.

[31] J. Canny, "A computational approach to edge detection," IEEE Transactions on Pattern Analysis and Machine Intelligence,Vol. PAMI-8, No. 6, 1986, pp. 679-698.

[32] Y. Xiao and H. Yan, “Facial feature location with delaunay triangulation/voronoi diagram calculation,” in Proceedings of the Pan-Sydney area workshop on Visual information processing 2001, Australian Computer Society, Inc., 2001, pp. 103–108.

[33] D. Silver, D. Ferguson, A. C. Morris, and S. Thayer, "Feature extraction for topological mine maps," Proceedings of the IEEE International Conference on Intelligent Robots and Systems (IROS), September, 2004, pp. 773 - 779.

[34] A. Fitzgibbon, M. Pilu and R. B. Fisher, "Direct least square fitting of ellipses", Pattern Analysis and Machine Intelligence, IEEE Transactions on Volume 21, Issue 5, May 1999 Page(s):476 – 480.

[35] R. Halir and J. Flusser, "Numerically stable direct least squares fitting of ellipses," 1998, in Skala, V (ed.) Proc. Int. Conf. in Central Europe on Computer Graphics, Visualization and Interactive Digital Media. 125--132.